

Ground-Moving Target Indication Using Along Track SAR Interferometer Designed with Triangular Frequency-Modulated Continuous Wave Radar

Young-Geun Kang, Seungwoon Park, Eunsung Kim, Jin-uk Lee, Kyeongrok Kim, Sangtae Kim,
and Seong-Ook Park, *Senior Member, IEEE*

Abstract—Synthetic aperture radar-ground-moving target indication (SAR-GMTI) system generates two-dimensional images of the observed area and detects moving targets within the image. Along track SAR interferometry (ATI) is gaining attention as a useful GMTI technique because it not only detects moving objects but also estimates the radial velocities of the detected objects. To unambiguously estimate the velocities of the moving objects with an ATI system, implementing a multi-baseline system with multi-channel is required, and frequency-modulated continuous wave (FMCW) radars are appropriate for multi-channel implementation due to their inherent bistatic properties. This paper proposes a practical and efficient SAR-GMTI design method that implements an ATI system with a triangular FMCW radar. The system is lightweight and affordable because it only requires a single FMCW radar. In addition, by adopting a triangular transmission signal model, the proposed system achieves the ability to distinguish signals for two channels in a single receiver. The usefulness of the proposed technique will be emphasized through comparison with the existing SAR-GMTI method using FMCW radars. Furthermore, the GMTI field test results using a van as a SAR platform are presented to demonstrate the validity of the proposed system. The experiment results of detecting multiple objects moving at various velocities validate the practicality of the proposed system. A method to verify the accuracy of the estimated velocities is also given.

Index Terms—Along track interferometry, frequency-modulated continuous wave, ground-moving target indication, synthetic aperture radar, triangular transmission model.

I. INTRODUCTION

SYNTHETIC aperture radar (SAR) generates two-dimensional images that express electromagnetic scattering information of the observed area. Unlike optical radar, SAR utilizes electromagnetic waves as an illumination source, making it usable regardless of climate and time conditions. Because of this all-time availability, SAR has been widely used for surveillance and earth observation applications. With the increasing demand for detecting moving objects in SAR images, various research has recently been conducted on SAR systems with ground-moving target indication (GMTI) capability [1-6]. GMTI techniques can be broadly categorized into single-channel and multi-channel approaches. Single-channel SAR detection methods include a range of approaches for moving target detection. One common approach involves utilizing the Doppler center frequency or Doppler slope to detect moving objects [7-8]. Another approach uses the compression level of the target's signal along with Doppler slope variations to distinguish moving targets [9]. While these methods are

computationally efficient, they are inherently less effective than multi-channel approaches in suppressing clutter, achieving high detection accuracy, and resolving velocity ambiguity [10]. Multi-channel SAR detection methods are primarily represented by displaced phase center antenna (DPCA) [11-13], space-time adaptive processing (STAP) [14-16], and along track SAR interferometry (ATI) [17-20].

DPCA detects moving targets by comparing phase signals from two or more spatially displaced antennas [21]. It is computationally efficient and effective for clutter cancellation. However, it may struggle in moving target detection in heterogeneous environments where clutter characteristics vary significantly [22]. Extended DPCA provides improved clutter cancellation capabilities by utilizing more phase centers and overcomes problems in heterogeneous environments, but often suffers from increased computational complexity and calibration challenges [12]. This complexity can limit its practical implementation and reliability. STAP is highly adaptive and enhances moving target detection performance even in complex cluttered environments because it performs signal processing simultaneously in both space and time domains. Nonetheless, it requires a substantial computational load and a significant training sample for effective clutter suppression [14]. Post-Doppler STAP reduces dimension and training samples to overcome the computational complexity issues in traditional STAP. However, it negatively impacts both clutter suppression and target detection performance due to residual range curvature problems [15]. ATI detects moving targets using the phase of interferogram generated from two SAR images with time differences in the along track direction. It is effective for detecting moving targets with small radar cross-sections (RCS), is less sensitive to channel mismatches, and requires less computation load compared to other GMTI methods [17], [41]. The authors have developed a practical and efficient SAR-GMTI system that is compatible with the ATI technique and capable of unambiguously estimating the velocity of the detected moving object.

Since conventional pulse radars are generally bulky and heavy, SAR-GMTI systems composed of pulse radars are hard to load on promising and small SAR platforms such as drones or unmanned aerial vehicles. Frequency-modulated continuous wave (FMCW) radar is expected to be a good alternative due to its relatively light and compact design. In addition, as FMCW radar is affordable in design cost and advantageous for obtaining high-resolution images through the

deramping technique, it has become a common radar for SAR. Accordingly, novel studies have been conducted to implement SAR-GMTI systems utilizing FMCW radars [23-25].

In [23-25], a theoretical method has been introduced that demonstrates the possibility of implementing GMTI with a single triangular FMCW radar [26-27], showing the potential for additional reduction in the design cost of the SAR-GMTI system. This existing method utilizes the fact that the range position of moving objects in FMCW SAR images varies depending on the sign of the frequency-modulation rate. However, the practicality of the method is strictly limited for several reasons. First, the difference in the range position of a moving object in the up-chirp and down-chirp FMCW SAR images is not large enough to be detected. Therefore, it is hard to detect moving objects, especially objects at low velocities. Second, because the actual location of the moving object is unknown in advance, it is essential to perform a visual inspection of the two SAR images to confirm the sign of the velocity of the moving object. This implies that the detection process is time-consuming and hard to automate. Furthermore, the resolution for the detectable velocity of the moving object is poor and discrete.

To overcome the aforementioned limitations of the existing method, we designed a practical and efficient triangular FMCW SAR-GMTI system. The proposed system utilizes a novel channel configuration technique that transmits up-chirp and down-chirp separately using two transmit antennas (TXs). This induces a time difference between the up-chirp and down-chirp SAR images, allowing the system compatible with the ATI technique. ATI is an efficient GMTI technique compared to the above method because the velocity is determined by the phase difference between two SAR images and therefore, is not limited to discrete value. By utilizing two TXs, each receiver generates two channels, enabling ATI function with just a single FMCW radar. Furthermore, utilizing the proposed technique makes it advantageous for multi-channel configurations, as adding just one more receiver allows for the implementation of a total of four channels. This means that a large number of channels can be implemented with fewer receivers, which will contribute to reducing the design cost and weight of the GMTI system.

To confirm the validity of the proposed SAR-GMTI system with real ATI data, we conducted an outdoor SAR-GMTI field test by mounting a quasi-4-channel Ku-Band triangular FMCW radar on the van. To the best of the author's knowledge, this article is the first literature demonstrating the detection results of actual moving objects with the ATI system implemented with the FMCW radar.

The rest of this paper is organized as follows. Section II reviews the existing moving target detection method using the triangular FMCW SAR-GMTI system and analyzes its limitations. It includes an analysis of the signal model of moving targets in the FMCW SAR image. In Section III, the proposed FMCW SAR-GMTI system design method using the ATI principle is introduced, and its usefulness is discussed. In addition, the reason why the triangular transmission model is recommended in the system design is presented. Section IV introduces the actual implementation of the proposed system

and the real moving object detection and velocity estimation results from actual ATI raw data. Also, a simple validation method is provided to verify the accuracy of the estimated velocities of the detected moving objects. The conclusion of this study is written in Section V.

II. EXISTING GMTI METHOD USING TRIANGULAR FMCW SAR

Fig. 1 shows the SAR data collection scenario where the moving object is present within the SAR illumination area. v is the radar platform velocity, \mathbf{v}_m is the object velocity, t_a is the azimuth time, x is the azimuth location of the radar, t_r is the range time, c is the speed of light, r is the slant range, and $P(r_0, x_0)$ is the location of the moving object when the radar is at $x = 0$. \mathbf{v}_m is the vector sum of the radial velocity v_r and the cross-range velocity v_x as follows:

$$\mathbf{v}_m = v_x \mathbf{X} - v_r \mathbf{r} \quad (1)$$

The v_x term in (1) is considered zero in this paper because its effect on the displacement or ATI phase of the moving object is little [21], [28]. Therefore, the radial velocity is expressed as velocity for brevity in the rest of this paper. In addition, it is assumed that v_r is much smaller than v because relatively fast objects are not compressed into SAR images due to severe Doppler shifts.

A. Signal Model of a Moving Target in FMCW SAR Image

A derivation process of the FMCW SAR model of a moving target is given in this subsection, and the detailed analysis of the conventional method and its limitations are discussed in the next subsection. From Fig. 1, the distance equation from the radar to the moving target approximates as follows [24]:

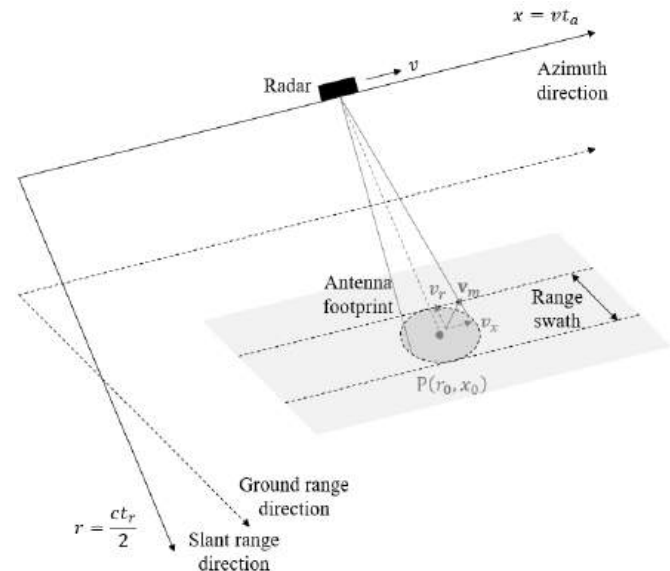


Fig. 1. SAR data collection scenario where the moving object is present.

$$r(t_r, t_a) = \sqrt{(r_0 - v_r t_a)^2 + (v t_a - x_0)^2} \approx r_0 - \frac{v_r}{v} x - v_r t_r + \frac{x^2}{2r_0} \quad (2)$$

A detailed derivation process of (2) is given in Appendix A. Note that the $v_r t_r$ term occurred because the stop-and-go approximation [29] is not applied in the derivation process. A complete moving object signal model in FMCW SAR image is given in (3). The basic Range-Doppler algorithm (RDA) is adopted as a SAR processing scheme [30].

$$s_o(f_r, t_a) = \text{sinc} \left[B_a \cdot \left(t_a - \frac{v_r}{v^2} r_0 \right) \right] \cdot \exp \left[-j \frac{4\pi v_r}{\lambda} t_a \right] \times \text{sinc} \left[T_r \cdot \left\{ f_r - \frac{2}{c} k_r \cdot \left(r_0 - \frac{r_0 v_r^2}{2v^2} - \frac{f_0 v_r}{k_r} \right) \right\} \right] \quad (3)$$

In (3), f_r is the range frequency, B_a is the Doppler bandwidth, λ is the radar wavelength, T_r is the duration of each pulse, k_r is the range frequency-modulation rate, and f_0 is the radar operating frequency. A detailed derivation process of (3) is given in Appendix B. To analyze the model in a spatial domain, it is rewritten as follows according to $x = v t_a$ and $r' = c f_r / (2k_r)$ relationships:

$$s_o(r', x) = \text{sinc} \left[\frac{1}{\rho_a} \cdot \left(x - \frac{v_r}{v} r_0 \right) \right] \cdot \exp \left[-j \frac{4\pi v_r}{\lambda v} x \right] \times \text{sinc} \left[\frac{1}{\rho_r} \cdot \left\{ r' - \left(r_0 - \frac{r_0 v_r^2}{2v^2} - \frac{f_0 v_r}{k_r} \right) \right\} \right] \quad (4)$$

where $\rho_a = v/B_a$ is the azimuth resolution and $\rho_r = c/(2k_r T_r)$ is the range resolution.

B. Conventional GMTI Method Using the Triangular FMCW SAR

As shown in (4), the azimuth and range displacements of the moving target in the FMCW SAR image are as follows, respectively:

$$\Delta x = \frac{v_r}{v} r_0 \quad (5)$$

$$\Delta r = \Delta r_1 + \Delta r_2 = -\frac{r_0 v_r^2}{2v^2} - \frac{f_0 v_r}{k_r} \quad (6)$$

By taking advantage of the fact that moving targets cause range displacement in the FMCW SAR model, a novel theoretical method has been introduced that demonstrates the possibility of implementing GMTI with a single FMCW radar, showing the potential for additional reduction in the design cost of the SAR-GMTI system [23-25]. The $\Delta r_1 = -r_0 v_r^2 / (2v^2)$ in (6) is a well-known range displacement value of the moving target that exists in the conventional pulsed SAR image also [21]. The $\Delta r_2 = -f_0 v_r / k_r$ in (6) is the additional range displacement value that exists only in the FMCW SAR image model, derived from the assumption that the stop-and-go approximation does not apply to FMCW SAR.

As this term is related to the k_r value, the displacement direction depends on the sign of k_r . Fig. 2 shows the channel configuration and a schematic diagram of the conventional triangular FMCW SAR-GMTI. Fig. 2(a) is given to compare it with the channel configuration of the proposed system in Section III. As shown in Fig. 2(b), the FMCW SAR systems utilizing a triangular linear frequency-modulated signal are able to generate two SAR images for the same observed area by applying the interferometric deformation technique [23-25]. One is generated from up-chirp, and the other is from down-chirp signals. The key idea of the conventional method is that the moving target is detectable in the interferogram because the moving target will be located in different range positions in the two SAR images due to the opposite sign of the additional range displacement. However, the practicality of this method is limited for the following reasons.

First, the system conditions for detecting moving targets are strictly limited. To identify a moving object by comparing the two SAR images, the difference between the additional range displacement values should exceed the range resolution of the SAR image. The corresponding condition is as follows:

$$\left| \frac{2f_0 v_r}{k_r} \right| > \left| \frac{c}{2k_r T_r} \right| \Rightarrow |v_r| > \frac{\text{PRF} \cdot \lambda}{2} = v_{min} \quad (7)$$

where v_{min} is the minimum velocity of a moving target required for detection and the PRF is the pulse repetition frequency of the radar. Unfortunately, in most FMCW SAR systems, the v_{min} value is too high to be used as a detection criterion because PRF and wavelength values are in a trade-off relationship. SAR systems with short radar wavelengths

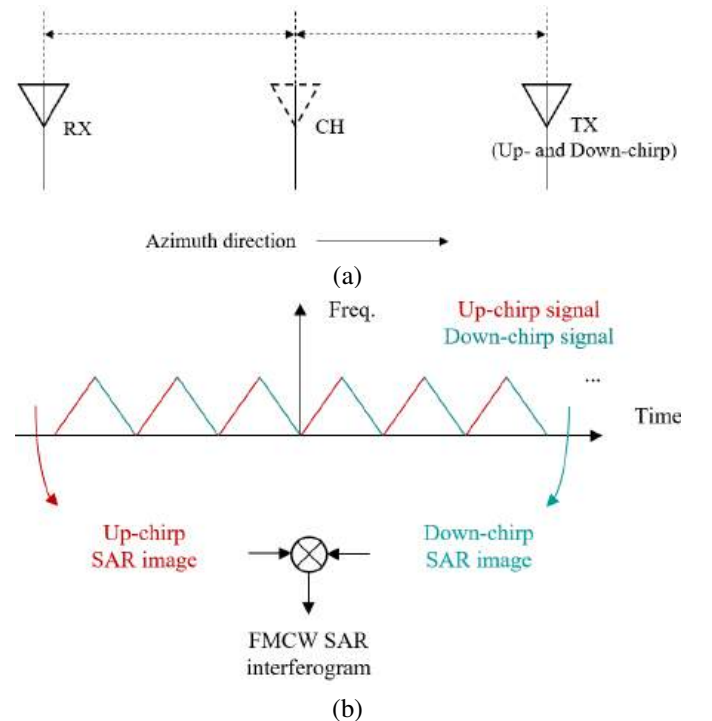


Fig. 2. (a) conventional channel configuration, (b) conventional GMTI method using triangular FMCW SAR.

lead to signals with wide Doppler bandwidth [31]. Otherwise, high system PRF values are required to process the wide bandwidth signals without aliasing. Table I shows several key specifications and corresponding v_{min} values for various practical FMCW SAR systems that are actually implemented [25], [30], [32-34]. The v_{min} values are high, making it difficult to detect slow targets. In addition, all of the FMCW SAR systems given in Table I have similar levels of v_{min} value to v , which contradicts the condition that the velocity of the object should be much smaller than the SAR platform velocity. That is, the moving targets will not be compressed appropriately within the SAR image before it reaches the minimum detectable velocity.

Second, it is impossible to determine the sign of the velocity of a moving target based solely on the interferogram of up-chirp and down-chirp FMCW SAR images. This is because in most cases, the radar has no prior knowledge of the actual position of the moving target. As shown in Fig. 3, the sign of the velocity of the detected moving target in the FMCW SAR interferogram cannot be determined until the positions of the object within the two SAR images are examined. This makes the detection process inefficient and hard to automate.

Finally, the resolution for the detectable velocity of the moving object is poor. In the conventional method, the velocity is estimated using the range pixel location difference between two SAR images, resulting in discrete estimates. The resolution for the detectable velocity is the same as the v_{min} value because the estimate varies only when the range location difference changes by the range resolution. It means that the resolution of the detectable velocity is not suitable for practical use.

TABLE I
SPECIFICATIONS OF VARIOUS PRACTICAL FMCW SAR SYSTEMS.

	v [m/s]	PRF [Hz]	λ [m]	v_{min} [m/s]
[25]	30	1000	0.03	16
[30]	20	5000	0.02	53
[32]	60	2895	0.03	45
[33]	45	3000	0.03	47
[34]	50	800	0.03	12

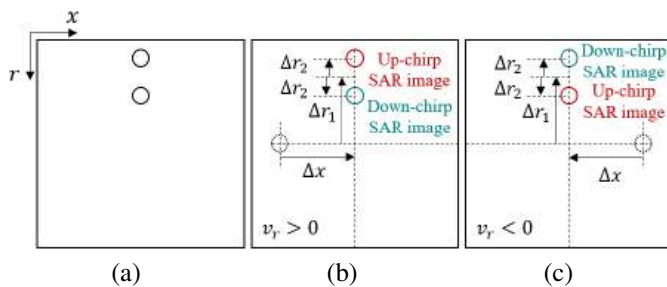


Fig. 3. An example of FMCW SAR interferogram and its corresponding two scenarios: (a) an FMCW SAR interferogram that detected a moving target, (b) case 1: the actual position of the moving target is on the left side of the SAR image and the velocity is positive, (c) case 2: the actual position of the moving target is on the right side of the SAR image and the velocity is negative.

III. PROPOSED TRIANGULAR FMCW SAR-GMTI USING ATI PRINCIPLES

As discussed in the previous section, detecting a moving target by the difference in the range position of the interferogram is impractical. This is because the moving target is detected only when the range position difference is wider than the range resolution, and the estimated velocity is updated only when the same amount of additional range position difference occurs. That is, the estimates are discrete. The reason the existing technique is impractical is because the Δr_2 value is too small. This term is derived from the assumption that stop-and-go approximation is not applicable to FMCW SAR. However, the applicability of the assumption is a controversial topic [35-38], and it has been discussed that it is generally applicable except in cases where the FMCW radar operates at frequencies over K-Band or the SAR platform velocity exceeds airplane levels (hundreds of m/s) [39]. Therefore, we assumed $v_r t_r$ in (2) is negligibly small, and accordingly, the equation (3) reduces as follows:

$$s_o(f_r, t_a) = \text{sinc} \left[B_a \cdot \left(t_a - \frac{v_r}{v^2} r_0 \right) \right] \cdot \exp \left[-j \frac{4\pi v_r}{\lambda} t_a \right] \times \text{sinc} \left[T_r \cdot \left\{ f_r - \frac{2}{c} k_r \cdot \left(r_0 - \frac{r_0 v_r^2}{2v^2} \right) \right\} \right] \quad (8)$$

where the $-f_0 v_r / k_r$ term is removed.

To develop a practical FMCW SAR-GMTI system, the authors focused on the fundamental bistatic characteristics of FMCW radars, allowing the system to be compatible with ATI principles. In this case, the estimates are continuous because the velocity is estimated from the phase of the interferogram.

Fig. 4 shows a basic ATI data acquisition scenario of a dual-channel case where a single baseline is implemented. Note that the two radars are spaced apart in the radar progression direction, with a baseline denoted as B_x . The baseline implies that there is a time difference in the azimuth direction in the two SAR images. As shown in the exponential term in (8), the phase of the SAR depends on the azimuth time and the velocity of the moving target. Therefore, the phase of the along track interferogram of the two SAR images with an azimuth

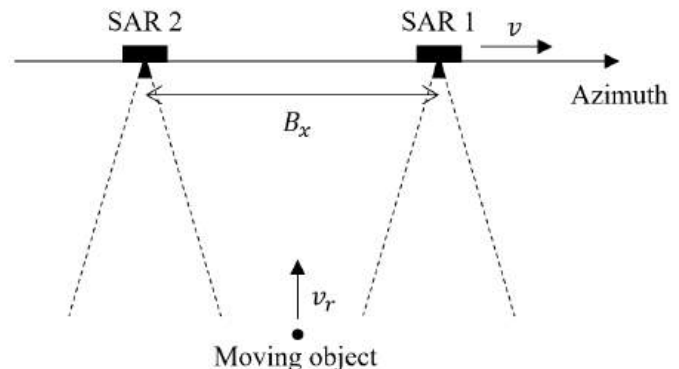


Fig. 4. A basic ATI data acquisition scenario of a dual-channel case (single baseline).

time difference contains the target velocity information. The ATI phase derived from (8) is as follows [40].

$$\begin{aligned} \phi_{ATI} &= \phi_{FORE}(t_a) - \phi_{AFT}(t_a + \Delta t) = \angle s_o(t_a) - \angle s_o(t_a + \Delta t) \\ &= -\frac{4\pi v_r}{\lambda} t_a - \left(-\frac{4\pi v_r}{\lambda} \cdot (t_a + \Delta t) \right) = \frac{4\pi v_r}{\lambda} \Delta t \quad (9) \end{aligned}$$

where ϕ_{FORE} and ϕ_{AFT} in (9) are the phases of the fore and aft radar SAR signal, respectively, and Δt is the azimuth time difference between the two SAR images.

We applied the ATI principle to a triangular FMCW radar to develop a practical SAR-GMTI system composed of a single radar. The key facts considered in developing the proposed system are as follows.

- 1) FMCW SAR systems utilizing the triangular transmission model are able to generate two SAR images for the same observed area. (Section II).
- 2) Two SAR images obtained with a slight time difference in the azimuth direction are required to detect the moving target and estimate its velocity (ATI principle).
- 3) The TX and the receive antenna (RX) are separated for continuous signal transmission and reception in the FMCW SAR system (Bistatic characteristic of FMCW radars).

In consideration of the above points, we propose a simple SAR-GMTI system design and antenna placement scheme, as shown in Fig. 5. The proposed system implements two transmission sources by using a switch to separate the up-chirp and down-chirp signals from the triangular signals, as shown in Fig. 5(a). To induce a time difference between the up-chirp and down-chirp SAR images, the down-chirp TX (TX2) should be placed in a delayed position in the azimuth direction relative to the up-chirp TX (TX1) as shown in Fig. 5(b). It is well-known that the TX and RX are individual and apart in the FMCW SAR system to continuously transmit and receive signals. The SAR signal obtained by the separated TX and RX is assumed to be equivalent to the SAR signal obtained by a virtual transceiver antenna (T/RX) located in the middle of TX and RX [21]. Therefore, the up-chirp SAR signal is assumed to be the same as the SAR signal obtained by the virtual T/RX (CH1) for TX1 and RX1, and the down-chirp SAR signal is assumed to be the same as the SAR signal obtained by the virtual T/RX (CH2) for TX2 and RX1. Then, the time difference between the two SAR images and the corresponding unambiguously detectable velocity v_{unamb} of the GMTI system are as follows:

$$\Delta t = \frac{B_{eq}}{v} = \frac{B_x}{2v} \quad (10)$$

$$|\phi_{ATI}| < \pi \Rightarrow |v_r| < \frac{\lambda v}{2B_x} = v_{unamb} \quad (11)$$

where B_{eq} is the equivalent baseline between virtual CHs. As shown in (11), since the phase is essentially a value restricted from $-\pi$ to π , ambiguity remains in the estimates when only a single baseline is implemented. The proposed system is advantageous to eliminate this ambiguity because it fully uses the bistatic property of the FMCW radar. By simply adding an additional single receiver (RX2) in the azimuth direction, two additional virtual T/RXs (CH3: TX1-RX2, CH4: TX2-RX2) are generated, allowing for the acquisition of three additional baselines (CH1-CH3, CH1-CH4, CH2-CH3) with different values.

On the other hand, the proposed system is theoretically replaceable with an FMCW radar that utilizes a sawtooth transmission model. However, using a sawtooth FMCW radar is not practical because it is difficult to distinguish between CH1 and CH2 signals from RX1. Most non-high-end radars require a certain amount of time from booting until data recording starts, and this duration is unpredictable. Sometimes more than a few seconds of delay occurs. This implies that the data recording start time will be from the middle point of the pulse. Therefore, in order for the proposed system to precisely separate the two channel signals from the receiver, the start time of the CH1 signal should be clearly identified.

Fortunately, most non-high-end radars suffer from flatness issues, which means they cannot generate signals of equal intensity for all frequencies when generating wide-bandwidth chirp signals. The triangular FMCW radars exploit this limitation in reverse, enabling the distinction between up-chirp (CH1) and down-chirp (CH2) signals based solely on the in-

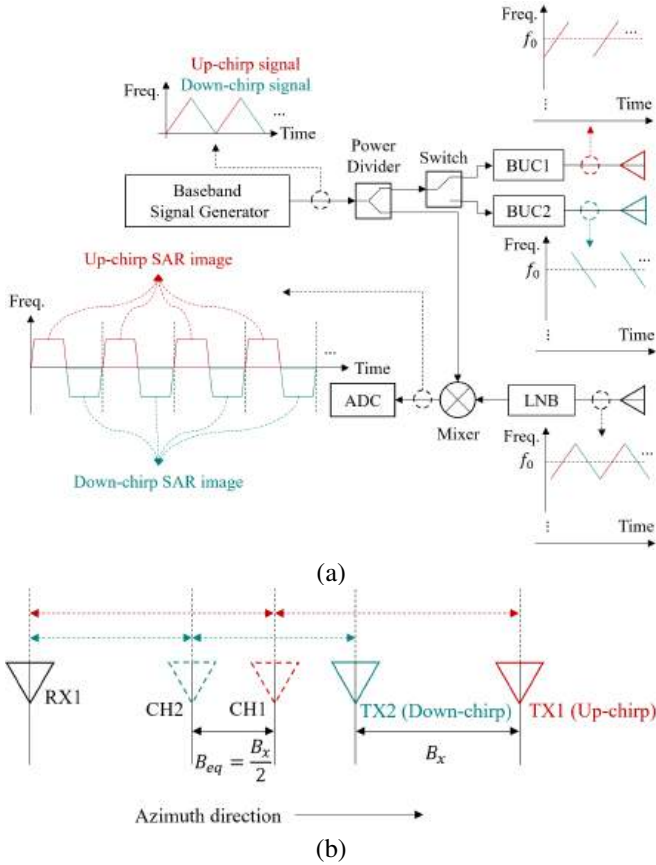


Fig. 5. Proposed SAR-GMTI system. (a) triangular FMCW radar design and signal flow diagram; (b) Placement scheme for transmit and receive antennas. The two dashed red and turquoise arrows are each the same length. The dashed red antenna is the virtual transceiver channel (CH) for TX1 and RX1. The dashed turquoise antenna is the virtual transceiver CH for TX2 and RX1. B_{eq} is the baseline between the CHs.

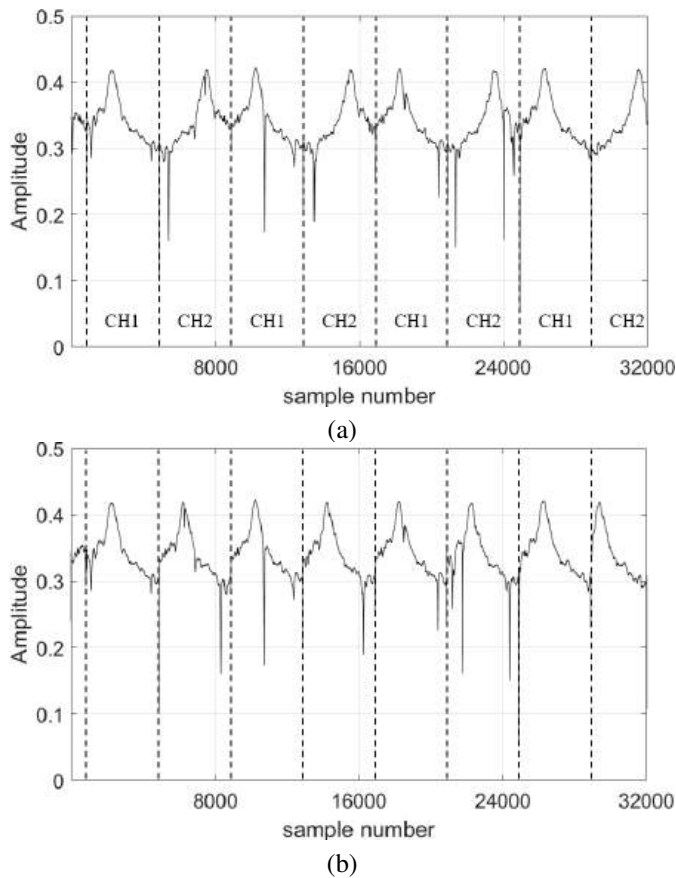


Fig. 6. Comparison of the intensity of the received signal according to transmission model. (a) triangular, (b) sawtooth.

tensity of the received signal waveform. However, the sawtooth radar that uses only up-chirp or down-chirp signals cannot take advantage of this property. Fig. 6 shows the comparison of the received signals corresponding to several consecutive pulse repetition intervals (PRI) according to the transmission model of FMCW radars. As shown in Fig. 6(a), using the triangular transmission model enables us to distinguish between CH1 and CH2 signals, allowing for precise determination of the starting point of the CH1 signal. However, utilizing the sawtooth transmission model makes it impossible to distinguish between CH1 and CH2 signals, thus preventing the accurate determination of the starting point of the CH1 signal.

IV. FMCW SAR-GMTI EXPERIMENT RESULTS

Section IV validates the proposed triangular FMCW SAR-GMTI system by presenting actual ATI raw data experiments. To achieve ATI raw data, the authors realized the proposed triangular FMCW SAR-GMTI system that is compatible with the ATI principle. As recommended in Section III, multiple baselines are implemented by using two receivers to remove ambiguity in the estimated velocities of the moving objects. Also, as this paper is one of the few reports that introduces actual moving target detection results using an ATI system utilizing FMCW radar, a method to prove the experiment results is also provided.



Fig. 7. A photo of SAR platform with the proposed SAR-GMTI system.

TABLE II
SPECIFICATIONS OF THE SAR-GMTI SYSTEM USED IN THE ACTUAL ATI EXPERIMENTS

Parameter	Value
Polarization	Linear (Vertical)
SAR platform velocity	80 km/h (22.22 m/s)
Transmission signal model	Triangular
Chirp Bandwidth	500 MHz
PRI	400 us
Radar center frequency	14.25 GHz
Radar wavelength	21.05 mm
The number of baselines	4
Equivalent baseline CH1-CH2	0.1 m
Equivalent baseline CH1-CH3	0.24 m
Equivalent baseline CH1-CH4	0.34 m
Equivalent baseline CH2-CH3	0.14 m

A. Experiment Scenarios and Results

Fig. 7 shows the photo of the TXs and RXs mounted on a van. Two receivers are used to implement 4 CHs and corresponding 6 baselines with four different values. To ensure accurate data acquisition, channel calibration was performed before the experiment. All hardware was synchronized using a common reference clock to ensure timing and phase alignment. In addition, a nearby corner reflector (CR) was used for phase calibration, improving phase delay and noise consistency across channels. The authors used a van for the SAR platform instead of a plane for financial issues. Note that using a plane is advantageous to detect faster-moving objects due to its high velocity.

The key specifications of the FMCW SAR-GMTI system and experiment parameters are listed in Table II. The Saedeul Bridge (Gongju, Republic of Korea) is adopted as the ATI test site. Because the Saedeul Bridge is a straight, long, and high bridge, it is suitable for SAR data acquisition. Fig. 8 shows the satellite image of the experiment site and implementation scenarios of moving and stationary objects. The authors took

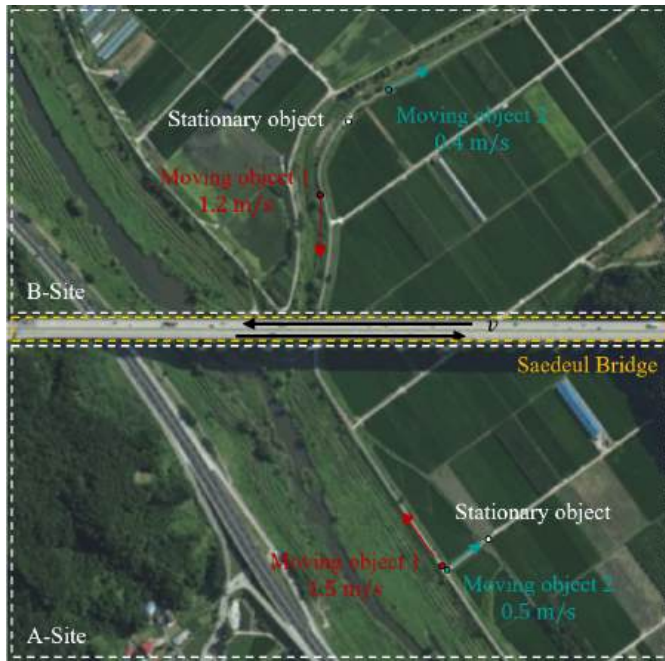


Fig. 8. A satellite image of the experiment site and implementation scenarios of moving and stationary objects.

SAR images of A and B sites while traveling back and forth the bridge and implemented two moving objects and one stationary object for each site. The signal-to-noise ratio at the selected experimental spots was measured to be over 20 dB, ensuring reliable data quality for the experiments. The authors adopted CRs to implement objects in the SAR images. As shown in Fig. 9, the stationary object is implemented by placing a CR on a tripod, and the moving objects are implemented by mounting the CRs on the automobile and trolley, respectively. As shown in the A-Site of Fig. 8, moving object #1 (MO #1) moved along the road at 1.50 m/s, corresponding to a radial velocity of 1.24 m/s, which is greater than the maximum unambiguously detectable velocity, 1.17m/s, when only the single baseline (CH1-CH2) is used. MO #2 moved along the road at 0.50 m/s, corresponding to a radial velocity of 0.28 m/s. In the B-Site, MO #1 and #2 moved along the road at 1.20 m/s and -0.40 m/s, corresponding to a radial velocity of 1.20 m/s and -0.24 m/s, respectively. The velocities of the moving objects are set to the above values to show that the proposed system is capable of detecting high- and low-velocity objects and resolving ambiguity in estimates.

Fig. 10 shows 4 FMCW SAR images and Fig. 11 shows corresponding 6 (${}_{4}C_{2}$) binary value images of the moving target detection results using along track interferograms. Note that the RDA for FMCW SAR is adopted for the SAR imaging algorithm, and the dual-threshold detection method in [40] is used for moving object detection. The dual-threshold scheme suppresses potential false alarms efficiently by applying both amplitude and phase thresholds sequentially. Especially, since we used CRs whose RCS is high to implement moving and stationary targets, the amplitude threshold could be set as a very high value. The moving target detection image results for the B-Site are omitted because the meaning of the results

TABLE III
VELOCITY ESTIMATION RESULTS FOR MOVING OBJECTS

A-Site		
	Moving object #1	Moving object #2
Theoretical (m/s)	1.24	0.28
Estimated (m/s)	1.20	0.26
B-Site		
	Moving object #1	Moving object #2
Theoretical (m/s)	1.20	-0.24
Estimated (m/s)	1.23	-0.23

is the same as the A-Site results. As shown in Fig. 10, the two moving objects and one stationary object appeared well in the SAR images. Since the radial velocity of a moving target causes an azimuth shift in SAR images as shown in (5), the two moving objects are slightly off the road in the azimuth direction. The binary value detection results in Fig. 11 show that all 6 along track interferograms only detected two moving objects. This implies that the dual-threshold detection method rejected the stationary target and many potential false alarms.

Table III summarizes the velocity estimation results of moving objects in A- and B-Site. A brief explanation for obtaining the estimated velocities is given as follows. Through Table II and (10), the azimuth time differences between channels are obtainable. Then, we are able to convert the measured phase from the along track interferograms to the velocities using the ATI phase equation in (9). For example, for the MO #1 in A-Site, the estimated velocities from the ATI phase between CHs are (CH1-CH2: -1.13 m/s, CH3-CH4: -1.16 m/s, CH1-CH3: 0.24 m/s, CH2-CH4: 0.22 m/s, CH1-CH4: -0.18 m/s, CH2-CH3: -0.46 m/s). These are ambiguous velocities since the phase is restricted from $-\pi$ to π . From (11), the candidates of actual velocity between CHs are (CH1-CH2: $\{\dots, -1.13, 0.04, \mathbf{1.21}, \dots\}$, CH3-CH4: $\{\dots, -1.16, 0.01, \mathbf{1.18}, \dots\}$, CH1-CH3: $\{\dots, 0.24, 0.73, \mathbf{1.21}, \dots\}$, CH2-CH4: $\{\dots, 0.22, 0.71, \mathbf{1.19}, \dots\}$, CH1-CH4: $\{\dots, -0.18, 0.16, 0.51, 0.85, \mathbf{1.20}, \dots\}$, CH2-CH3: $\{\dots, -0.46, 0.38, \mathbf{1.21}, \dots\}$). We obtained the estimated velocity of 1.20 m/s as the average of the bolded values, which are the intersection of the candidates. The proposed SAR-GMTI system estimated velocities of moving objects within about 7% error. The error might have been caused by various factors, such as inaccuracies and inconsistencies in implementing the SAR platform and moving object velocities. The authors implemented the desired velocities depending on the speed instrument panel for the SAR platform (van) and the MO #1 (automobile). For the MO #2 (trolley), it was roughly implemented by dividing the travel distance by the SAR integration time. Also, the presence of clutter and noise signals would have caused the error [41].

From (11) and Table II, the maximum unambiguously detectable velocity is 1.17 m/s when only a single baseline is used. Because the proposed system implemented multiple



Fig. 9. Stationary and moving objects. (a) stationary object, (b) moving object #1 (automobile), (c) moving object #2 (trolley).

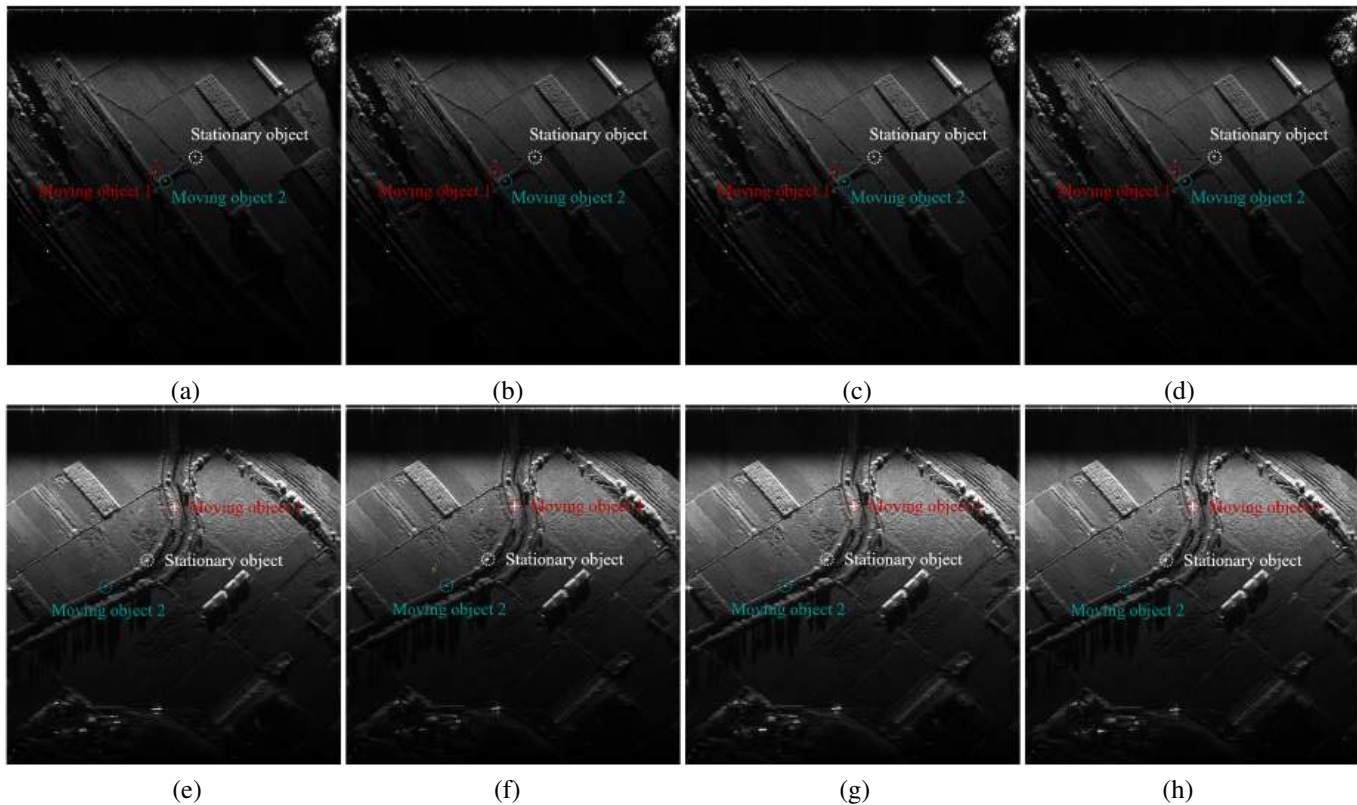


Fig. 10. 4-Channel FMCW SAR images. (a) CH1 (A-Site), (b) CH2 (A-Site), (c) CH3 (A-Site), (d) CH4 (A-Site), (e) CH1 (B-Site), (f) CH2 (B-Site), (g) CH3 (B-Site), (h) CH4 (B-Site).

baselines using 2 receivers, it could resolve the ambiguity in estimates, and therefore, could accurately estimate the velocity of MO #1, whose velocity is greater than 1.17 m/s.

Note that, the estimates are all zero when the existing GMTI technique is used because the difference in range displacement is much smaller than range resolution. This result demonstrates that configuring the SAR-GMTI system to be compatible with the ATI principle is more practical.

B. Verification of the ATI Experiment Results

This subsection introduces a method to prove the estimated moving object velocity results. As shown in (5) and Fig. 10, the moving object is displaced in the azimuth direction within the SAR image. As given in Table II, the radar platform velocity in the experiment was fixed at about 22.22 m/s. The measured ranges of the moving objects were 277.8 m (MO #1 in A-Site), 292.8 m (MO #2 in A-Site), 169.8 m (MO #1 in B-Site), and 302.7 m (MO #1 in B-Site), respectively.

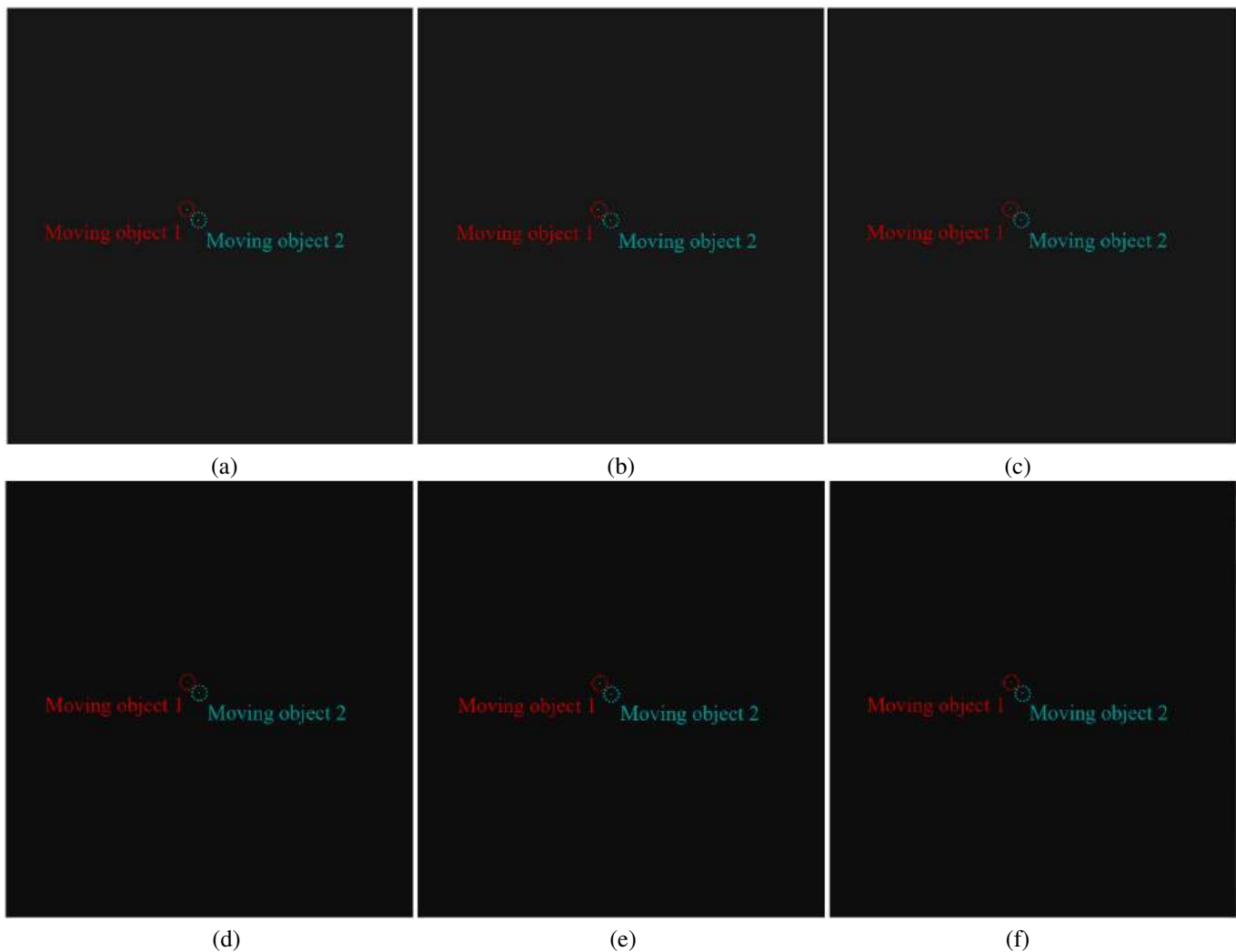


Fig. 11. 6 binary value images of the moving object detection results (A-Site). (a) CH1-CH2, (b) CH1-CH3, (c) CH1-CH4, (d) CH2-CH3, (e) CH2-CH4, (f) CH3-CH4.

According to the estimated radial velocities of the moving objects in Table III and the azimuth displacement equation in Eq. (5), the moving objects in the FMCW SAR image should be coordinated by about 15.00 m (MO #1 in A-Site), 3.43 m (MO #2 in A-Site), 9.40 m (MO #1 in B-Site), and -3.13 m (MO #1 in B-Site), respectively. Enlarged SAR images where the locations of the moving objects are corrected are shown in Fig. 12. As shown in Fig. 12, all moving objects have been accurately calibrated onto the road, indicating that the estimates are valid. This result proves that the FMCW SAR-GMTI using the ATI technique is practical.

V. CONCLUSION

This paper proposed a design method for the SAR-GMTI system using a single triangular FMCW radar. The existing triangular FMCW SAR-GMTI system transmits both up-chirp and down-chirp signals with a single TX and therefore, it is not compatible with the ATI method. Therefore, the existing system uses the range position differences between the up-chirp and down-chirp SAR images to detect the moving

targets, but this has been discussed as impractical. To be compatible with the ATI technology, the proposed system utilizes two TXs to separately transmit up-chirp and down-chirp signals. One TX is arranged at a position delayed from the other TX in the along-track direction to induce a time difference between the up-chirp and down-chirp SAR images. It was also discussed why the triangular waveform should be used from a practical perspective. Note that the proposed channel configuration technique is hard to apply to pulse radars because pulse radars generally transmit a much higher power compared to FMCW radars. When multiple TXs are used, the leakage signal from one TX to another TX is too strong. Therefore, separately transmitting up-chirp and down-chirp signals using 2 TXs is not recommended in pulse SAR. Compatible with ATI functionality, the proposed system detects moving objects based on phase differences rather than range position differences, resulting in the estimation of the continuous value of the moving target velocity. In addition, it has the advantage of being able to configure multiple channels just by adding another receiver. It is expected to be widely

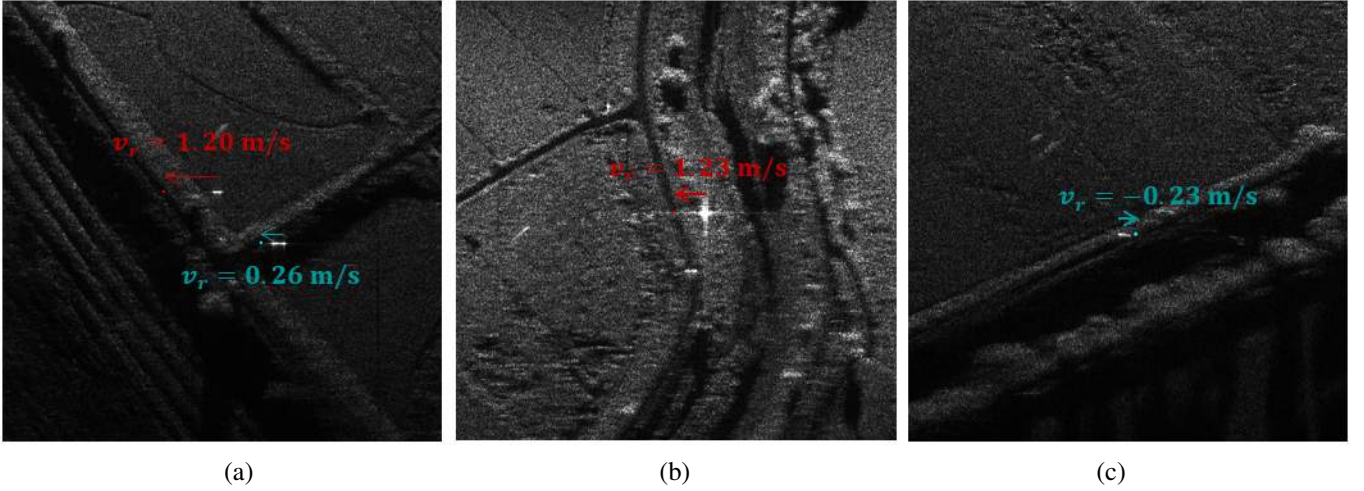


Fig. 12. Enlarged SAR images where the locations of the moving objects are corrected. (a) MO #1 and #2 (A-Site), (b) MO #1 (B-Site), (c) MO #2 (B-Site).

used for its inexpensive design cost and to be applied to future SAR platforms such as drones for its lightweight and compact configuration.

In addition, the authors demonstrated the validity and practicality of the proposed system by conducting actual ATI raw data experiments. In particular, it is meaningful in terms of practicality verification that, as far as the authors know, this paper is the first literature to report the results of actually performing ATI experiments with an FMCW radar. However, because the conducted experiment utilized a van as a SAR platform, verification for faster-moving objects was limited due to the requirement that the platform velocity should be significantly faster than the moving target velocity. Using satellites or airplanes as SAR platforms will enable system verification for faster objects, such as vehicles running on highways. The authors expect that this study will contribute to the popularization of the FMCW SAR-GMTI system using ATI principles.

APPENDIX

A. Range Equation Between a Radar and a Moving Target

Appendix A shows a detailed derivation of the approximation of the range equation between the radar and the moving object.

$$\begin{aligned}
 r(t_a) &= \sqrt{(r_0 - v_r t_a)^2 + (v t_a - x_0)^2} \\
 &= \sqrt{r_0^2 + x_0^2 - 2 \cdot (r_0 v_r + v x_0) \cdot t_a + (v_r^2 + v^2) \cdot t_a^2} \\
 &= \sqrt{r_0^2 + x_0^2} \cdot \left[1 - \frac{2 \cdot (r_0 v_r + v x_0)}{r_0^2 + x_0^2} t_a + \frac{v_r^2 + v^2}{r_0^2 + x_0^2} t_a^2 \right]^{\frac{1}{2}} \\
 &\approx \sqrt{r_0^2 + x_0^2} \cdot \left[1 - \frac{r_0 v_r + v x_0}{r_0^2 + x_0^2} t_a + \frac{1}{2} \cdot \frac{v_r^2 + v^2}{r_0^2 + x_0^2} t_a^2 \right. \\
 &\quad \left. - \frac{1}{2} \cdot \frac{(r_0 v_r + v x_0)^2}{(r_0^2 + x_0^2)^2} t_a^2 \right] \quad (\text{A.1})
 \end{aligned}$$

The approximation notation at the bottom of (A.1) is derived from the third-order Taylor equation [42]. Assuming a

broadside mode ($x_0 = 0$), (A.1) is reduced as follows without loss of generality.

$$r(t_a) = r_0 - v_r t_a + \frac{v^2}{2r_0} t_a^2 = r_0 - \frac{v_r}{v} x + \frac{x^2}{2r_0} \quad (\text{A.2})$$

Note that (A.2) is the range equation with the stop-and-go approximation. Without the stop-and-go approximation, (A.2) is modified as follows because the radar moves during the signal transmission and reception.

$$\begin{aligned}
 r(t_r, t_a) &= r_0 - v_r t_a + \frac{v^2}{2r_0} t_a^2 \\
 &= r_0 - v_r \cdot (T_n + t_r) + \frac{v^2}{2r_0} \cdot (T_n + t_r)^2 \\
 &\approx r_0 - v_r T_n + v_r t_r + \frac{v^2}{2r_0} T_n^2 \\
 &= r_0 - \frac{v_r}{v} x_n + v_r t_r + \frac{x_n^2}{2r_0} \quad (\text{A.3})
 \end{aligned}$$

where $T_n = n \cdot \text{PRI}$ is the discrete azimuth time variable with n integer and $x_n = v T_n$ is the discrete azimuth position variable of the SAR platform. PRI is the abbreviation for pulse repetition interval. (A.3) is resulted to (2) by replacing x_n with x for simplicity [24].

B. Detailed Derivation Process of the Moving Target Signal Model in FMCW SAR Image

The intermediate signal de-ramped at the receiver of the FMCW radar is as follows:

$$\begin{aligned}
 s_{IF}(t_r, t_a) &= \text{rect} \left[\frac{t_r}{T_r} \right] \cdot \text{rect} \left[\frac{t_a}{T_{syn}} \right] \\
 &\quad \times \exp[j2\pi \cdot (f_0 \tau(t_r, t_a) + k_r \tau(t_r, t_a) t_r)] \quad (\text{B.1})
 \end{aligned}$$

where T_r is the duration of each pulse, T_{syn} is the synthetic aperture time, f_0 is the radar operating frequency, k_r is the range frequency-modulation rate, and $\tau(t_r, t_a) = 2r(t_r, t_a)/c$

is the time takes for the signal to round trip the moving object. The exponential term in (B.1) is rewritten as follows:

$$\begin{aligned}
 & \exp[j2\pi \cdot (f_0\tau(t_r, t_a) + k_r\tau(t_r, t_a)t_r)] \\
 &= \exp\left[j\frac{4\pi}{\lambda}r(t_r, t_a)\right] \cdot \exp\left[j\frac{4\pi}{c}k_r t_r r(t_r, t_a)\right] \\
 &= \exp\left[j \cdot \left(\frac{4\pi}{\lambda} + \frac{4\pi}{c}k_r t_r\right) \cdot \left(r_0 - \frac{v_r}{v}x + \frac{x^2}{2r_0}\right)\right] \\
 &\times \exp\left[-j \cdot \left(\frac{4\pi}{\lambda} + \frac{4\pi}{c}k_r t_r\right) \cdot v_r t_r\right] \\
 &\approx \exp\left[j \cdot \left(\frac{4\pi}{\lambda} + \frac{4\pi}{c}k_r t_r\right) \cdot \left(r_0 - \frac{v_r}{v}x + \frac{x^2}{2r_0}\right)\right] \\
 &\times \exp\left[-j\frac{4\pi}{\lambda}v_r t_r\right] \tag{B.2}
 \end{aligned}$$

The approximation notation at the bottom of (B.2) is valid for narrow-bandwidth cases. The rewriting is continued as follows:

$$\begin{aligned}
 & \exp[j2\pi \cdot (f_0\tau(t_r, t_a) + k_r\tau(t_r, t_a)t_r)] \\
 &= \exp\left[j \cdot \left(\frac{4\pi}{\lambda} + \frac{4\pi}{c}k_r t_r\right) \cdot \left(r_0 - \frac{v_r}{v}x + \frac{x^2}{2r_0}\right)\right] \\
 &\times \exp\left[-j\frac{4\pi}{c}k_r t_r \frac{f_0 v_r}{k_r}\right] \\
 &= \exp\left[j\frac{4\pi}{\lambda} \cdot \left(r_0 - \frac{v_r}{v}x + \frac{x^2}{2r_0}\right)\right] \\
 &\times \exp\left[j\frac{4\pi}{c}k_r t_r \cdot \left(r_0 - \frac{v_r}{v}x + \frac{x^2}{2r_0} - \frac{f_0 v_r}{k_r}\right)\right] \tag{B.3}
 \end{aligned}$$

By using (B.3), the range Fourier transformed (FFT) signal of (B.1) is as follows:

$$\begin{aligned}
 S_{IF}(f_r, t_a) &= \text{rect}\left[\frac{t_a}{T_{syn}}\right] \cdot \exp\left[j\frac{4\pi}{\lambda} \cdot \left(r_0 - \frac{v_r}{v}x + \frac{x^2}{2r_0}\right)\right] \\
 &\times \text{sinc}\left[T_r \cdot \left\{f_r - \frac{2}{c}k_r \cdot \left(r_0 - \frac{v_r}{v}x + \frac{x^2}{2r_0} - \frac{f_0 v_r}{k_r}\right)\right\}\right] \tag{B.4}
 \end{aligned}$$

where f_r is the range frequency. It is well known that the sinc function is the range signal. The azimuth FFT and range cell migration corrected signal of (B.4) is as follows:

$$\begin{aligned}
 S(f_r, f_a) &= \text{rect}\left[\frac{f_a + 2v_r/\lambda}{B_a}\right] \cdot \exp\left[-j\frac{\pi}{k_a} \cdot \left(f_a + \frac{2v_r}{\lambda}\right)^2\right] \\
 &\times \text{sinc}\left[T_r \cdot \left\{f_r - \frac{2}{c}k_r \cdot \left(r_0 - \frac{r_0 v_r^2}{2v^2} - \frac{f_0 v_r}{k_r}\right)\right\}\right] \tag{B.5}
 \end{aligned}$$

where f_a is the azimuth frequency, k_a is the azimuth frequency-modulation rate, B_a is the Doppler bandwidth. Note that the principle of stationary phase [42] technique is used to implement azimuth FFT. The final FMCW SAR image signal model (3) is obtained by implementing the azimuth-matched filtering and inverse azimuth FFT on the signal (B.5).

ACKNOWLEDGMENT

This work was supported by Institute of Information & Communications Technology Planning & Evaluation(IITP) grant funded by the Korea government(MSIT) (No.2018-0-01658, Key Technologies Development for Next Generation Satellites) and a grant-in-aid of HANWHA SYSTEMS.

REFERENCES

- [1] P. Huang *et al.*, "Imaging and Relocation for Extended Ground Moving Targets in Multichannel SAR-GMTI Systems," in *IEEE Transactions on Geoscience and Remote Sensing*, vol. 60, pp. 1-24, 2022, Art no. 5214024.
- [2] Z. Yang, H. Xu, P. Huang, A. Liu, M. Tian, and G. Liao, "Preliminary Results of Multichannel SAR-GMTI Experiments for Airborne Quad-Pol Radar System," in *IEEE Transactions on Geoscience and Remote Sensing*, vol. 58, no. 6, pp. 3822-3840, June 2020.
- [3] C. Han, Z. Yang, G. Liao, Q. Zhang, S. He, and H. Xu, "A SAR-GMTI Approach Aided by Online Knowledge With and Airborne Multichannel Quad-Pol Radar System," in *IEEE Journal of Selected Topics in Applied Earth Observations and Remote Sensing*, vol. 15, pp. 8668-8681, 2022.
- [4] Z. Zhang, D. Wu, D. Zhu, and Y. Zhang, "A Multichannel SAR Ground Moving Target Detection Algorithm Based on Subdomain Adaptive Residual Network," in *IEEE Geoscience and Remote Sensing Letters*, vol. 20, pp. 1-5, 2023, Art no. 4010705.
- [5] A. Vafaei, M. Modarres-Hashemi, and S. J. Zahabi, "GMTI and GMTIm via Fractional Fourier Transform and GLRT in SAR," in *IEEE Transactions on Instrumentation and Measurement*, vol. 72, pp. 1-8, 2023, Art no. 8505908.
- [6] J. K. Jao, "Target Signal-to-Noise Loss in Multichannel SAR-GMTI Clutter Suppression," in *IEEE Transactions on Aerospace and Electronic Systems*, vol. 59, no. 6, pp. 9463-9479, Dec. 2023.
- [7] J. R. Moreira and W. Keydel, "A new MTI-SAR approach using the reflectivity displacement method," in *IEEE Transactions on Geoscience and Remote Sensing*, vol. 33, no. 5, pp. 1238-1244, Sept. 1995.
- [8] S. V. Baumgartner and G. Krieger, "Fast GMTI algorithm for traffic monitoring based on a priori knowledge," in *IEEE Transactions on Geoscience and Remote Sensing*, vol. 50, no. 11, pp. 4626-4641, Nov. 2012.
- [9] R. D. Chapman, C. M. Hawes, and M. E. Nord, "Target Motion Ambiguities in Single-Aperture Synthetic Aperture Radar," in *IEEE Transactions on Aerospace and Electronic Systems*, vol. 46, no. 1, pp. 459-468, Jan. 2010.
- [10] E. Makhoul, A. Broquetas, J. Ruiz Rodon, Y. Zhan, and F. Cebe, "A Performance Evaluation of SAR-GMTI Missions for Maritime Applications," in *IEEE Transactions on Geoscience and Remote Sensing*, vol. 53, no. 5, pp. 2496-2509, May 2015.
- [11] Y. Hou, J. Wang, X. Liu, K. Wang, and Y. Gao, "An automatic SAR-GMTI algorithm based on DPCA," *2014 IEEE Geoscience and Remote Sensing Symposium*, Quebec City, QC, Canada, 2014, pp. 592-595.
- [12] D. Cerutti-Maori and I. Sikaneta, "A Generalization of DPCA Processing for Multichannel SAR/GMTI Radars," in *IEEE Transactions on Geoscience and Remote Sensing*, vol. 51, no. 1, pp. 560-572, Jan. 2013.
- [13] S. Wacks and B. Yazıcı, "Bistatic Doppler-SAR DPCA imaging of ground moving targets," *2014 IEEE Radar Conference*, Cincinnati, OH, USA, 2014, pp. 1071-1074.
- [14] W. L. Melvin, "A STAP overview," *IEEE Aerospace and Electronic Systems Magazine*, vol. 19, no. 1, pp. 19-35, Jan. 2004.
- [15] J. Chen, D. An, B. Ge, and Z. Zhou, "Detection, Parameters Estimation, and Imaging of Moving Targets Based on Extended Post-Doppler STAP in Multichannel WasSAR-GMTI," *IEEE Transactions on Geoscience and Remote Sensing*, vol. 62, pp. 1-15, 2024, Art no. 5223515.
- [16] C. D. Peckham, A. M. Haimovich, T. F. Ayoub, J. S. Goldstein, and I. S. Reid, "Reduced-rank STAP performance analysis," *IEEE Transactions on Aerospace and Electronic Systems*, vol. 36, no. 2, pp. 664-676, April 2000.
- [17] E. Chapin and C. W. Chen, "Airborne along-track interferometry for GMTI," *IEEE Aerospace and Electronic Systems Magazine*, vol. 24, no. 5, pp. 13-18, May 2009.
- [18] R. M. Goldstein and H. A. Zebker, "Interferometric radar measurement of ocean surface currents," *Nature*, vol. 328, pp. 707-709, Aug. 1987.
- [19] R. M. Goldstein, T. P. Barnett, and H. A. Zebker, "Remote sensing of ocean currents," *Science*, vol. 246, no. 4935, pp. 1282-1285. 1989.

- [20] E. Chapin and C. W. Chen, "Along-track interferometry for ground moving target indication," in *IEEE Aerospace and Electronic Systems Magazine*, vol. 23, no. 6, pp. 19-24, June 2008.
- [21] S. V. Baumgartner, and G. Krieger, "Multi-Channel SAR for Ground Moving Target Indication," Elsevier: Amsterdam, The Netherlands, 2014, vol. 2, pp. 911-986.
- [22] A. Budillon, C. H. Gierull, V. Pascazio, and G. Schirinzi, "Along-Track Interferometric SAR Systems for Ground-Moving Target Indication: Achievements, Potentials, and Outlook," *IEEE Geoscience and Remote Sensing Magazine*, vol. 8, no. 2, pp. 46-63, June 2020.
- [23] A. Meta, "Signal Processing of FMCW Synthetic Aperture Radar Data," Ph.D. thesis, Delft University of Technology, Holland, 2005.
- [24] A. Meta and P. Hoogeboom, "Signal processing algorithms for FMCW moving target indicator synthetic aperture radar," in *Proc. IEEE Int. Geosci. Remote Sens. Symp.*, Seoul, Korea (South), 2005, pp. 1-4.
- [25] A. Meta, P. Hoogeboom, and L. P. Ligthart, "Signal processing for FMCW SAR," in *IEEE Transactions on Geoscience and Remote Sensing*, vol. 45, no. 11, pp. 3519-3532, Nov. 2007.
- [26] Z. Duan, Y. Wu, M. Li, W. Wang, Y. Liu, and S. Yang, "A Novel FMCW Waveform for Multi-target Detection and the Corresponding Algorithm," *2017 IEEE 5th International Symposium on Electromagnetic Compatibility*, Beijing, China, 2017, pp. 1-4.
- [27] A. Bazzi, M. Ghareeb, M. Raad, and S. Abdul-Nabi, "Movement detection using a modified FMCW waveform and GNU radio," in *International Journal of Engineering Research & Technology (IJERT)*, vol. 6, no. 4, Apr. 2017.
- [28] A. Budillon, V. Pascazio, and G. Schirinzi, "Estimation of Radial Velocity of Moving Targets by Along-Track Interferometric SAR systems," in *IEEE Geoscience and Remote Sensing Letters*, vol. 5, no. 3, pp. 349-353, July 2008.
- [29] R. Lorusso and G. Milillo, "Stop-and-go approximation effects on COSMO-SkyMed spotlight SAR data," *2015 IEEE International Geoscience and Remote Sensing Symposium (IGARSS)*, Milan, Italy, 2015, pp. 1797-1800.
- [30] D.-H. Jung, H.-S. Kang, C.-K. Kim, J. Park, and S.-O. Park, "Sparse scene recovery for high-resolution automobile FMCW SAR via scaled compressed sensing," *IEEE Trans. Geosci. Remote Sens.*, vol. 57, no. 12, pp. 10136-10146, Dec. 2019.
- [31] I. G. Cumming and F. H. Wong, *Digital Processing of Synthetic Aperture Radar Data: Algorithms and Implementation*. Norwood, MA, USA: Artech House, 2005.
- [32] H. Bi, J. Zhang, P. Wang, and G. Bi, "Airborne FMCW SAR sparse data processing via frequency scaling algorithm," *IEEE Geoscience and Remote Sensing Letters*, vol. 18, no. 7, pp. 1224-1228, 2021.
- [33] H. Bi, J. Wang, and G. Bi, "Wavenumber domain algorithm-based FMCW SAR sparse imaging," *IEEE Trans. Geosci. Remote Sens.*, vol. 57, no. 10, pp. 7466-7475, 2019.
- [34] Y. Liu, Y. Deng, and R. Wang, "Focus squint FMCW SAR data using inverse chirp-Z transform based on an analytical point target reference spectrum," *IEEE Geoscience and Remote Sensing Letters*, vol. 9, no. 5, pp. 866-870, 2012.
- [35] A. Meta and P. Hoogeboom, "High resolution airborne FM-CW SAR: digital signal processing aspects," in *Proceedings of 2003 IEEE International Geoscience and Remote Sensing Symposium*, Toulouse, France, 2003, pp. 4074-4076.
- [36] J. J. de Wit, A. Meta, and P. Hoogeboom, "Modified range-Doppler processing for FM-CW synthetic aperture radar," *IEEE Geoscience and Remote Sensing Letters*, vol. 3, no. 1, pp. 83-87, 2006.
- [37] B. Wang, Z. Hu, W. Guan, Q. Liu, and J. Guo, "Study on echo signal model and RD imaging algorithm for FMCW SAR," in *Proceedings of IET International Radar Conference*, Hangzhou, China, 2015, pp. 1-6.
- [38] E. Casalini, M. Frioud, D. Small, and D. Henke, "Refocusing FMCW SAR moving target data in the wavenumber domain," *IEEE Transactions on Geoscience and Remote Sensing*, vol. 57, no. 6, pp. 3436-3449, 2019.
- [39] Y.-G. Kang, D.-H. Jung, G.-H. Shin, C.-K. Kim, and S.-O. Park, "A study on the feasibility of stop-and-go approximation in FMCW SAR," *J. Electromagn. Eng. Sci.*, vol. 22, no. 3, pp. 210-217, May 2022.
- [40] Y. Zhang, "Along track interferometry synthetic aperture radar (ATI-SAR) techniques for ground moving target detection," Defense Technical Information Center, AFRL-SN-RS-TR-2005-410, Jan. 2006.
- [41] C. W. Chen, "Performance assessment of along-track interferometry for detecting ground moving targets," *Proceedings of the 2004 IEEE Radar Conference*, Philadelphia, PA, USA, 2004, pp. 99-104.
- [42] R. K. Raney, "A New and Fundamental Fourier Transform Pair," *1992 IEEE International Geoscience and Remote Sensing Symposium (IGARSS)*, Houston, 1992, pp. 106-107.



Young-Geun Kang was born in Daejeon, South Korea, in February 1994. He received the B.S. degree in electrical and electronic engineering from Yonsei University, Seoul, South Korea, in 2018, and the M.S., and Ph.D. degrees in electrical engineering from Korea Advanced Institute of Science and Technology (KAIST), Daejeon, South Korea, in 2020, and 2024, respectively.

He has been a principal research engineer at the radar recognition logic cell, Hyundai Mobis, Yongin, Republic of Korea, since March 2024. His research interests include synthetic aperture radar (SAR), radar systems, and radar data processing.



Seungwoon Park received the B.S. and M.S. degrees in electrical engineering from the Korea Advanced Institute of Science and Technology, Daejeon, South Korea, in 2016 and 2018, where he is currently pursuing the Ph.D. degree in electrical engineering.

His current research interests include frequency-modulated continuous-wave radar systems for Synthetic Aperture Radar and SAR interferometry.



Eunsung Kim was born in Nonsan, South Korea, in 1996. He received the B.S. degree from Korea University, Seoul, South Korea, in 2022. He is currently studying for his Ph.D. in Electrical Engineering at the Korea Advanced Institute of Science and Technology in Daejeon, South Korea.

His current research interests include radar systems and radar signal processing.



Jin-uk Lee received the B.S. degree in electronics engineering from Pusan National University, Busan, South Korea, in 2022, and the M.S. degree in electrical engineering from Korea Advanced Institute of Science and Technology (KAIST), Daejeon, South Korea, in 2024, where he is currently pursuing the Ph.D. in electrical engineering.

His current research interests include the design of frequency modulated continuous wave radar systems and radar signal processing.



Kyeongrok Kim (Member, IEEE) has been a senior engineer at the Satellite System 2 Team, Hanwha Systems, Yongin, Republic of Korea, since February 2022. He received his M.S., and Ph.D. degrees in department of space electronics and information technology and electrical and computer engineering from Ajou University, Suwon, Republic of Korea, in 2016, and 2022, respectively.

His current research interests include design and development of small synthetic aperture radar (SAR) satellite, SAR performance analysis, and SAR image processing. He was a recipient of Best Paper Award by KICS (2017), Bronze Paper Award from IEEE Seoul Section Student Paper Contest (2018), Director Award by Korea Electronics Technology Institute (2020), Participation Award by Electronic Times ICT Paper Contest (2020), Grand Prize by Haedong Paper Award from KICS (2021), Best Paper Award by from Ajou University Graduate School (2022).



Sangtae Kim has been an engineer at the Satellite System 2 Team, Hanwha Systems, Yongin, Republic of Korea, since August 2022. He received his M.S. degrees in department of avionics engineering from Korea Aerospace University, Goyang, Republic of Korea, in 2018.

His current research interests include design and development of small synthetic aperture radar (SAR) satellite, SAR performance analysis, and SAR Antenna system.



Seong-Ook Park (Senior Member, IEEE) received the B.S. degree from KyungPook National University, KyungPook, Korea, in 1987, and the M.S. degree from Korea Advanced Institute of Science and Technology (KAIST), Daejeon, in 1989, and the Ph.D. degree from Arizona State University, Tempe, in 1997, under the supervision of Professors Constantine A. Balanis.

From March 1989 to August 1993, he was a Research Engineer with Korea Telecom, Daejeon, working with microwave systems and networks. He later joined the Telecommunication Research Center, Arizona State University, until September 1997.

He is a member of Phi Kappa Phi Scholastic Honor Societies. He has been a member of the faculty at the Information and Communications University from October 1997 to 2008, and has been currently a full professor since 2009 at KAIST. He has over 200 publications in refereed journals. He served as the Director General, Satellite Technology Research Center, KAIST from 2016 to 2018. He also served as President of The Korean Institute of Electromagnetic Engineering and Science (KIEES) in 2022. He has studied the improvement of antenna function inside of handset platforms, analytical and numerical techniques in the area of electromagnetics wave, and the precision technique of antenna measurement. His main focus is on the drone detection radar, SAR Payload, and the antenna system.